



Accurate determination of the shapes of granular charge distributionsNicolás Mujica ¹ and Scott Waitukaitis ²¹*Departamento de Física, Facultad de Ciencias Físicas y Matemáticas, Universidad de Chile, Avenida Blanco Encalada 2008, Santiago, Chile*²*Institute of Science and Technology Austria, Lab Building West, Am Campus 1, 3400 Klosterneuburg, Austria*

(Received 20 September 2022; accepted 17 February 2023; published 8 March 2023)

Experiments have shown that charge distributions of granular materials are non-Gaussian, with broad tails that indicate many particles with high charge. This observation has consequences for the behavior of granular materials in many settings, and may bear relevance to the underlying charge transfer mechanism. However, there is the unaddressed possibility that broad tails arise due to experimental uncertainties, as determining the shapes of tails is nontrivial. Here we show that measurement uncertainties can indeed account for most of the tail broadening previously observed. The clue that reveals this is that distributions are sensitive to the electric field at which they are measured; ones measured at low (high) fields have larger (smaller) tails. Accounting for sources of uncertainty, we reproduce this broadening *in silico*. Finally, we use our results to back out the true charge distribution without broadening, which we find is still non-Gaussian, though with substantially different behavior at the tails and indicating significantly fewer highly charged particles. These results have implications in many natural settings where electrostatic interactions, especially among highly charged particles, strongly affect granular behavior.

DOI: [10.1103/PhysRevE.107.034901](https://doi.org/10.1103/PhysRevE.107.034901)**I. INTRODUCTION**

The electrostatic charging of granular materials is important in many natural settings. In thunderclouds, dust storms, and volcanic plumes, grain charging helps to generate lightning [1]. In industry, charge-driven coagulation hinders grain transport [2], or can lead to explosions [3]. Charged dust in clean rooms sullies sensitive samples, but permits extraction during electrostatic precipitation [4]. Outside of these terrestrial settings, charged dust adheres to and damages spacecraft on planets, moons, or asteroids [5], and may even be implicated in the formation of rocky planets [6].

In order to understand, and especially to model [7,8], the effects of grain charging, one must have some knowledge of the extent to which grains are charged. Ideally the distribution of charges should be known, but in most situations this is not possible. Geophysicists chasing naturally charged granular media, e.g., dust storms [9] or volcanic plumes [10], can gather some rough data about charge, but not distributions that can be easily reproduced. For astrophysical situations, experiments to measure charge are currently impossible. Pertinent to any of these situations, however, an alternative approach is to measure grain charge distributions in laboratory experiments [6,11–14]. Though often carried out under different conditions and utilizing different materials, such experiments uniformly reveal charge distributions with non-Gaussian tails [6,12,13,15], which are important for several reasons. First, these tails imply large numbers of highly-charged particles, which can strongly affect how the grains interact. Second, though not the focus of this paper, the tails may bear relevance to the underlying mechanism for charge transfer [16–19].

The aim of this work is to accurately determine the shape of granular charge distributions. We use the technique with which the most complete distributions thus far have been

gathered, i.e., videographic particle tracking of charged grains in response to an external electric field [6,12,13,15]. Using an improved version of this method, we obtain distributions from measurements of up to hundreds of thousands of individual grains. Like previous experiments, we too observe non-Gaussian tails, but with an important new piece of information: the shape depends on the applied electric field. Specifically, tails measured with small fields are broader than those measured with large fields. Considering that virtually no charge-exchanging collisions occur while particles are in the field, we investigate the possibility that field-dependence is related to uncertainties inherent to the videographic technique. We find this is indeed a significant source of broadening, and illustrate how the mechanism occurs by creating charge distributions *in silico* and broadening them via subjection to the same correlated sources of uncertainty present in experiments. Ultimately, we find that accurate charge distributions can be obtained, but only if measured at sufficiently large fields and accounting for this synthetic broadening.

II. EXPERIMENTAL PROCEDURE

We follow the method of Ref. [12] for particle charge measurements by free-fall videography, as illustrated in Fig. 1(a). Particles are loaded into a hopper at the top of a ~ 2 m vacuum chamber, which is evacuated to a pressure of 4×10^{-4} mbar via a rotary-vane roughing pump and a turbopump. At the beginning of each experiment, a nozzle ($D_n = 14.5$ particle diameters) at the bottom of the hopper is opened, allowing the particles to fall freely as a dilute stream. A high-speed camera (Phantom v641, 2560×1600 pix², 1456 fps) initially held focused on the nozzle, is released to fall with a segment of the stream, guided by low-friction rails and protected below with foam padding. Shortly after leaving the nozzle, the particles enter a region of uniform external electric field, created by

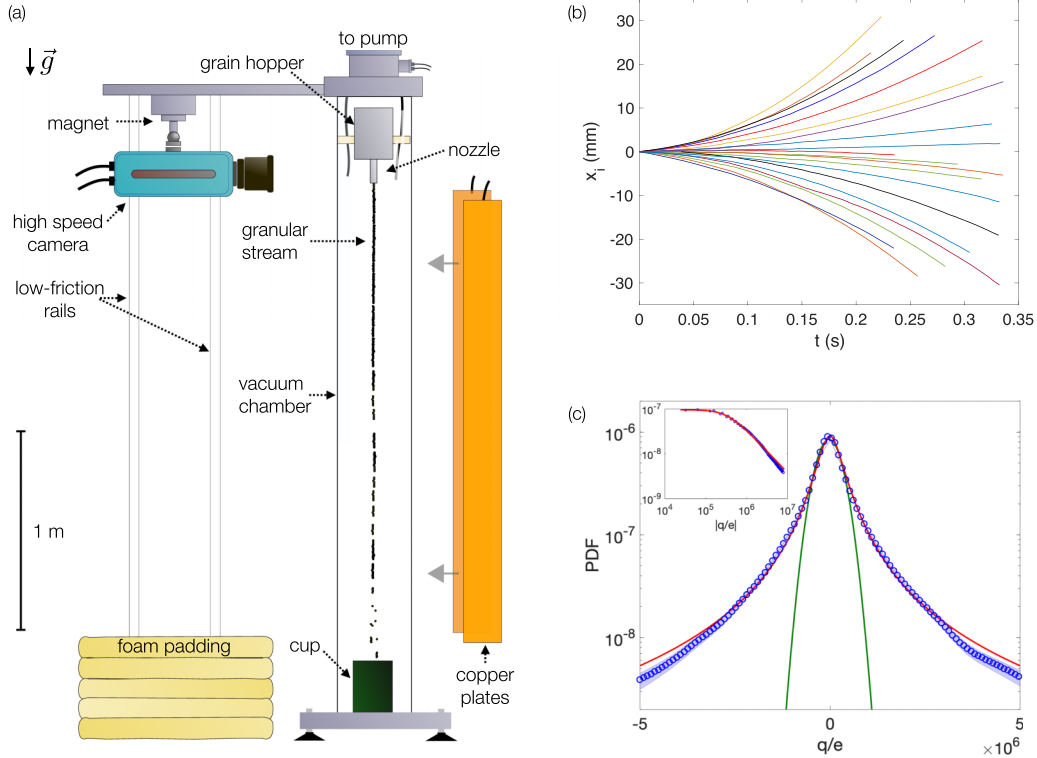


FIG. 1. (a) Experimental system. A high speed camera falls along low friction rails while watching a cofalling stream of granular particles. The particles are accelerated into/out of the page by an electric field across two copper plates (drawn outside chamber for clarity). (b) Examples of particle trajectories in the horizontal direction at an applied field of 150 kV/m. (c) Measured charge distribution for $|\mathbf{E}| = 90$ kV/m, with uncertainty bands obtained as mentioned in the text. The solid green curve is the Gaussian fit of the central peak. The solid red line is the phenomenological fit to Eq. (1). The inset shows the same data/fit on a double logarithmic scale.

applying a voltage, V , between two tall (1.8 m) copper plates connected to the chamber side walls (separation $L = 0.1$ m). We track the horizontal trajectories of particles in response to this field to measure their charge. To correct for lateral movements of the camera, we use a vertical string hung at the back of the chamber as a reference, as in Ref. [12]. The string is attached to a metallic rod forming a pendulum, which is damped at the bottom via submersion in a high-viscosity liquid. In addition to the string correction, we further refine removal of global movement by subtracting the average deviation of particle positions from fitted trajectories. We use the same particles as Ref. [12]; $\text{ZrO}_2\text{:SiO}_2$ particles (65:35 composite, Glenn Mills Inc.) from an initially broad size distribution are sieved to reach a final distribution that is almost monodisperse, with an average diameter $D = 299.8 \pm 11.5$ μm as determined by optical microscopy.

Examples of corrected trajectories are shown in Fig. 1(b), where the parabolic shapes of charged particles in response to a uniform field are observed. As a sanity check, we have confirmed that analyzing trajectories with the same method as Ref. [12] reveals largely identical results. However, for this manuscript we analyze trajectories with the method of Ref. [6]. We convert each individual acceleration measurement (extracted by fitting the parabolic trajectories) to charge via $q_i = a_i \bar{m} / |\mathbf{E}|$. Here, $\bar{m} = (5.4 \pm 0.3) \times 10^{-8}$ kg is the average mass, as deduced from the microscopy images and assuming a mass density $\rho = 3800$ kg/m³. We assign this same mass to all particles because the resolution in the exper-

iment is not sufficient to accurately determine each particle’s size separately. An example probability distribution function (PDF) is presented in Fig. 1(c) for a field strength of $|\mathbf{E}| = 90$ kV/m. We obtain confidence intervals for such a PDF (shaded region in figure) by considering the uncertainty of each acceleration measurement, deploying a Monte Carlo algorithm which randomly picks new values for each acceleration from within its uncertainty range to create alternative distributions, from which we can calculate each bin’s standard deviation. Like previous experiments, we see non-Gaussian tails at both positive and negative q , which surround a Gaussian central portion. Previous experiments [6, 14] fit their tails to exponential behavior. If we fit our data in Fig. 1(c) over the range $|q| \in [0.83, 2.25] \times 10^6 e$ to the exponential functions $e^{\beta_{l,r} q}$, we obtain $\beta_l = 1.29 \pm 0.06$ and $\beta_r = -1.31 \pm 0.06$. These exponents are comparable to Ref. [6], who measured exponents 1.24 and -0.96 for the left/right sides, respectively, though with a different material (glass). However, with our larger data set, we find that the tails are much better approximated by power-law behavior, not exponential. Empirically, we find the entire distribution fits well to the function

$$F(q) = \frac{F_o}{[1 + (|q|/\Delta_q)^\alpha]}, \quad (1)$$

where F_o is a measure of the distribution’s maximum, Δ_q quantifies its width, and α captures the limiting power-law behavior [red solid line in Fig. 1(c) and inset].

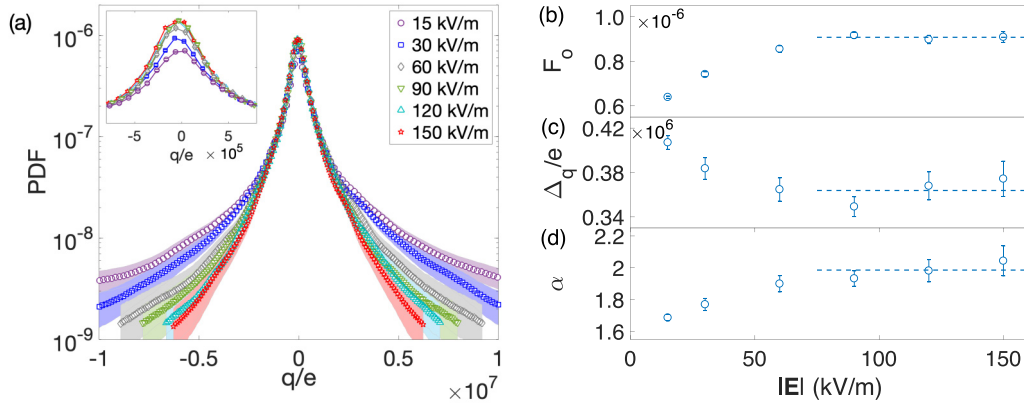


FIG. 2. (a) Charge PDFs for all data from the field-sweep experiments plotted together on a semilog scale. The non-Gaussian tails appear to change with the electric field, as well as the PDF maximum value (figure inset). (b) Charge PDF maximum value F_0 , (c) characteristic distribution width Δ_q and (d) limiting power law exponent α , respectively, vs the electric field $|\mathbf{E}|$. All quantities tend to converge to constant values for the largest $|\mathbf{E}|$. The dashed lines show the averages of the last three values. The quantities F_0 , Δ_q , and α are obtained from fits to Eq. (1), as shown in Fig. 1(c).

III. DEPENDENCE OF TAILS ON THE APPLIED ELECTRIC FIELD

We now investigate what happens to distributions when the field is changed. Plots of the PDF for a sweep of fields ($|\mathbf{E}| \in \{15, 30, 60, 90, 120, 150\}$ kV/m) are shown in Fig. 2(a). For each field, the distributions are comprised of approximately 22,000 individual measurements. This field-sweep data reveals two important trends. First, the maximum values around $|q| = 0$ are lower for lower fields (see inset). Second, the PDFs for larger fields have less pronounced tails. These two features are expected to occur simultaneously since the PDFs are normalized. The fact that the error bands of these distributions do not overlap indicates that the differences in their shapes as the field is changed are significant. However, we do observe that for the larger fields, the PDFs tend to collapse on a single curve, at least for larger ranges of $|q|$.

We characterize the evolution of the distribution shape by fitting at each field the PDF to Eq. (1), from which we obtain F_0 , Δ_q , and α , as shown in Figs. 2(b)–2(d). Error bars correspond to the 95% confidence interval of each adjusted parameter. All three parameters change quickly for low fields, but begin to saturate at approximately 90 kV/m. These data illustrate in particular that the power-law behavior of the tails changes with the field at which the measurement is done. At low fields, $\alpha \approx 1.6$, while at high fields it seems to saturate at approximately two. Practically, this means there appear to be far more highly charged particles in distributions taken at low fields vs high fields. For example, particles with a charge of $>6 \times 10^6 e$ appear to be nearly $10\times$ more prevalent in the 15 kV/m data as compared to the 150 kV/m data.

IV. CONNECTION OF THE FIELD-DEPENDENCE TO EXPERIMENTAL UNCERTAINTIES

One might naïvely suspect that field-dependence reflects changes to the underlying charge distribution, as several works indicate that collisional charge exchange is driven or at least influenced by the presence of external fields [20–22].

Continual collisions, sliding, and rolling do occur when particles are inside the hopper, however during this stage they are shielded from the applied electric field by the hopper’s metallic walls. On the other hand, when the grains exit the hopper and enter the region where the electric field is applied, virtually no collisions occur. Therefore, barring some exotic mechanism that would be hard to motivate, it is more reasonable to presume that the underlying charge distribution is unchanged by the field.

We therefore pursue a different hypothesis, namely that the field evolution is a manifestation of uncertainties inherent to the measurement technique. The simplified argument for how this works is as follows. First, suppose an ensemble of grains has some underlying charge distribution, $P(q)$. If we put these grains in the experiment and measure their trajectories at zero applied field, we would *not* measure an acceleration distribution of zero width. Instead, it would have finite width due to the fact that each acceleration measurement is not perfect—uncertainties in the tracked position and the finite lifetimes of the grains cause each acceleration measurement to have an uncertainty. Since $q = ma/E$, converting this finite-width acceleration distribution to charge would yield an *infinite* width, despite the actual distribution having finite width. For finite electric fields, vestiges of this mechanism can persist, hence leading to finitebroadening of the measured charge distribution compared to the actual one.

Accounting for this properly is not as simple as the argument above suggests. If all acceleration measurements had the same uncertainty, then the actual charge distribution could be recovered through deconvolution of the measured acceleration distribution with the acceleration uncertainty. However, the acceleration uncertainties are not the same for all particles, and in fact exhibit correlations with other relevant parameters. The most prominent of these is in Fig. 3(a), where we plot the acceleration uncertainties as a function of the particle lifetimes, i.e., how long they are tracked before exiting the video. As these data show, particles tracked for longer durations have smaller uncertainties than those tracked for shorter

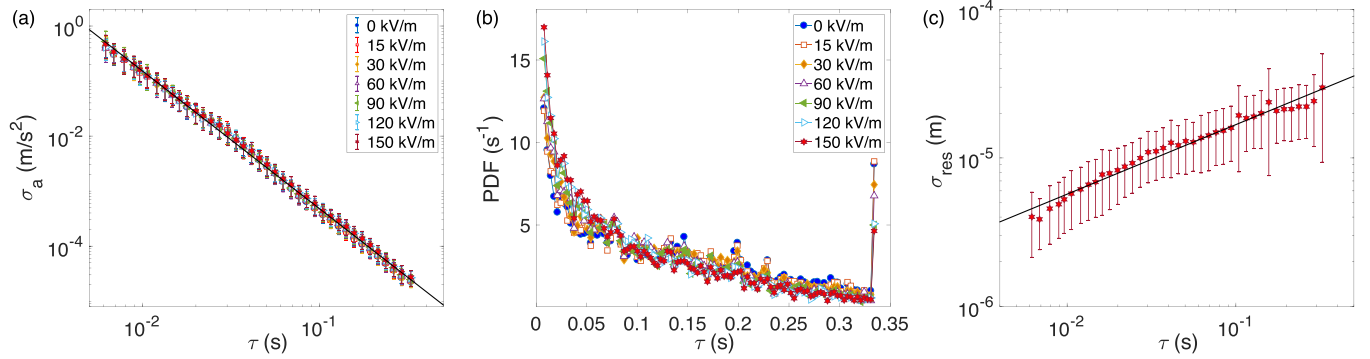


FIG. 3. (a) Acceleration uncertainty, σ_a , plotted against lifetime, τ , for all $|\mathbf{E}|$. The data have been windowaveraged in 39 bins. Error bars correspond to the standard deviation of the data of each bin. A decreasing power law behavior is obtained, $\langle \sigma_a \rangle = D\tau^\epsilon$. As there is no $|\mathbf{E}|$ dependence, we merge all the data together to fit and obtain $\epsilon = -2.50 \pm 0.01$ and $D = (1.500 \pm 0.015) \times 10^{-6} \text{ m s}^{1/2}$, shown with the continuous black line. (b) Particle lifetime PDF, also for all fields. The peak at the maximum trajectory lifetime, $\tau_{\text{max}} = 0.3359 \text{ s}$, corresponds to those trajectories that remain tracked throughout the complete video acquisition (490 frames at 1456 fps). Again there is no field dependence. (c) Tracked position residuals standard deviation, σ_{res} , versus lifetime, τ , for the highest field $|\mathbf{E}| = 150 \text{ kV/m}$. We also checked that there is no field dependence. These residuals ultimately cause the acceleration uncertainties in (a), and they are also correlated to the lifetime through a power law. For the window-averaged data, we get $\langle \sigma_{\text{res}} \rangle = C\tau^\delta$, with $\delta = 0.47 \pm 0.03$ and $C = (4.93 \pm 0.04) \times 10^{-5} \text{ m s}^{-\delta}$, shown with the continuous black line.

durations, obeying a power law exponent of -2.5 . The data are subdivided based on field, illustrating that there is no field-dependence to this trend. The second important observation is shown in Fig. 3(b), namely that the distribution of lifetimes is not uniform—many more particles are tracked for short lifetimes than for long ones. This feature is also essentially independent of the strength of the field. These trends indicate that, ultimately, the acceleration uncertainties arise due to positional tracking uncertainty. In Fig. 3(c), we plot the standard deviation of the tracked position residuals vs lifetime, which illustrates that these, too, are correlated. To properly account for how uncertainties affect the tails of charge PDFs, all of these factors must be considered simultaneously.

V. REPRODUCTION OF BROADENED TAILS BY ADDING EXPERIMENTAL NOISE AND CORRELATIONS INTO SYNTHETIC DATA

Based on the arguments and observations of the previous section, we now illustrate *in silico* how uncertainties can broaden an underlying charge distribution. We do this accounting for the correlations between the quantities involved. We start by numerically generating a set of “particles” with whatever charge PDF we would like. For each “particle”, we assign a mass, drawn from the mass distribution determined from optical microscopy, and a lifetime from the experimental lifetime distribution [Fig. 3(b)]. Next, for each particle we generate a corresponding “pristine” trajectory. We then add noise to each of these trajectories based on the residuals standard deviations of Fig. 3(c). With these “dirty” trajectories, we then analyze exactly as in the experiments, namely: (1) fit each trajectory to obtain an acceleration a_i , (2) convert this acceleration into a charge via $q_i = a_i \bar{m} / |\mathbf{E}|$ (again using the average mass, since in experiments individual masses cannot be obtained *in situ*), and (3) from these q_i calculate charge PDFs.

In Fig. 4 we show what happens when an input Gaussian charge distribution of the form,

$$F_G(q) = \frac{1}{\sqrt{2\pi}\sigma_q} \exp\left[-\frac{q^2}{2\sigma_q^2}\right], \quad (2)$$

is subjected to this process, and in particular as a function of the applied field. As is clear, the recovered charge distribution is always broadened compared to the input one, and this broadening becomes worse and worse as the applied field becomes smaller. If we plot the PDF maxima and limiting behavior of the tails, as in Figs. 4(b)–4(d), we see qualitatively similar behavior as in the experiment: the maxima increases with field, the width decreases, and the power-law exponent at the extremes of the tails becomes larger, although in this case with no saturation at high $|\mathbf{E}|$. We thus conclude that this “uncertainty broadening” is sufficient to explain the field-dependence of tails observed in experiments.

VI. DETERMINING THE TRUE UNDERLYING SHAPE OF AN EXPERIMENTAL DISTRIBUTION

With understanding of the broadening mechanism, we reconsider our experimental data. We first consider whether or not an underlying Gaussian charge distribution can be broadened to reproduce an experimental distribution. To test this, we note that, given the mean charge of experimental distributions is close to zero, a potential underlying Gaussian would be a function of a single parameter, namely the width, σ_q . We can therefore compare a computergenerated and broadened input Gaussian distribution to an experimental one to see, as a continuous function of σ_q , when it best represents the experiment. To define “best”, we calculate the χ^2 difference between the output of the numerically generated distribution and the experimental one. The plot of χ^2 vs σ_q is shown in Fig. 5(a), where the experimental data chosen are at $|\mathbf{E}| = 150 \text{ kV/m}$ and the simulation is run at this same value. As can be seen,

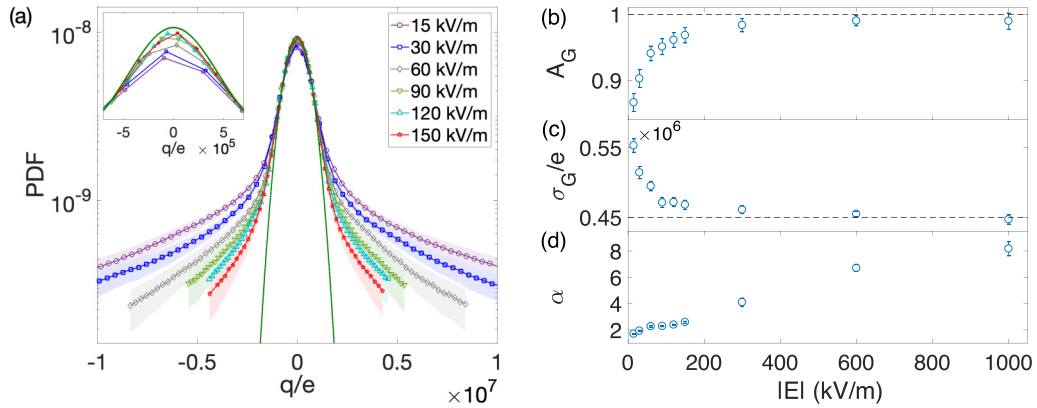


FIG. 4. (a) Charge PDFs for the simulation data of an input Gaussian charge distribution, with $\sigma_q = 0.45 \times 10^6 e$, as the electric field is increased. The inset shows the detail around the distribution maxima for fields up to 150 kV/m, as in the experiment. In panels (b), (c), and (d) we plot the PDF maximum, width, and limiting power, respectively, similar to the experimental data of Figs. 2(b)–2(d). The shapes of these distributions are not fitted well by Eq. (1), hence we use a slightly different approach to extract these values. For panels (b) and (c), we fit the central peak to a Gaussian, $A_G/(\sqrt{2\pi}\sigma_G) \exp[-q^2/(2\sigma_G^2)]$, where the factor A_G gives the PDF maximum and σ_G characterizes the width. For the limiting power law behavior, we extend the field dependence up to 1000 kV/m and simply fit the tails to a power law. Contrary to experiments, α does not converge to a fixed value. This is consistent with the fact that the underlying PDF is a Gaussian. The dashed lines in panels (b) and (c) show the original charge distribution values for $A_G = 1$ and $\sigma_q = 0.45 \times 10^6 e$.

there is a clear optimum when the input Gaussian distribution has a width of $\sigma_q \approx 0.45 \times 10^6 e$. However, even though this is the optimum, Fig. 5(b) shows that it is an extremely poor one—it does not replicate the experimental data. As we explain in the caption to Fig. 5, we cannot satisfactorily fit Gaussian simulated data to Eq. (1), further verifying its lack of correspondence to experiments. We therefore reaffirm the widespread conclusion that the underlying charge distribution is not Gaussian.

Can an underlying non-Gaussian distribution fair better? Part of the difficulty of this question is knowing *which* non-Gaussian distribution to pick, as there are limitless options. We take a clue from our experimental data of Figs. 2(b)–2(d), where the maximum, width, and limiting powers of the distributions saturate at sufficiently large fields. Based on these observations, we assume that the charge distribution measured at the highest fields is approximately the correct one, and

we therefore use this as a guess for our input distribution. Using this as our input distribution and subjecting it to the uncertainty broadening is a stringent test, as it effectively “double broadens” the true underlying charge distribution—once from the analysis of the experiment, and once from inserting it into our numerical routine. Nonetheless, we see in Fig. 5(c) that this double-broadened distribution is, within our calculated uncertainty bands, indistinguishable from the experimental result. Hence we can conclude that at sufficiently high fields, experiments can recover the underlying charge distribution.

VII. DISCUSSION AND CONCLUSIONS

Taken together, our work leads us to reaffirm the generality of non-Gaussian tails in granular charge distributions, but with the caveat that extracting the true shape is more complicated

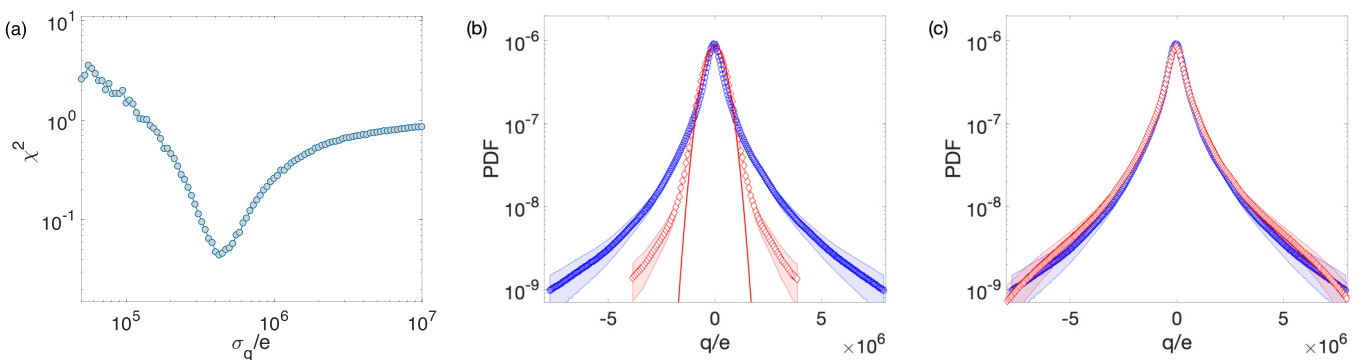


FIG. 5. (a) Objective function χ^2 vs charge distribution width σ_q in log-log scale. A clear minimum is observed at $\sigma_q = (0.45 \pm 0.01) \times 10^6 e$. (b) Comparison of the best simulation charge PDF (red \diamond), obtained with zero mean and $\sigma_q = 0.45 \times 10^6 e$, with the experimental one (blue \circ), both for $|\mathbf{E}| = 150$ kV/m. The continuous red line shows the analytical charge PDF used in the simulation. As is clear, even this “best Gaussian” is wholly inadequate to explain experimental data. (c) Simulation (red \diamond) and experimental (blue \circ) charge PDF for $|\mathbf{E}| = 150$ kV/m. We generate the former by using experimental data at the highest fields as our input charge distribution and subjecting it to the noise sources as described in the text.

than might otherwise be expected. The key observation that has been missing is that the shape of charge distributions depends on the field strength, with broad tails being more pronounced at smaller fields. Given that there is, to our knowledge, no evidence that grains acquire charge in vacuum in the absence of collisions, the most reasonable cause we can propose for the observed behavior is measurement uncertainty. By numerically generating artificial charge distributions from known input distributions subjected to our observed uncertainty correlations and statistics, we recreate the observed broadening. Our tests to see if an underlying Gaussian distribution can replicate our experimental data reveal that, even in the best case scenario, it cannot. On the other hand, we show that effectively subjecting high-field experimental data to the uncertainty broadening twice does not lead to a significant

change in its shape; hence, we conclude that at sufficiently high fields the correct underlying charge distribution can be obtained.

ACKNOWLEDGMENTS

This research was supported by Grants QUIMAL 160001 and Fondecyt 1221597. This project has received funding from the European Research Council (ERC) under the European Union's Horizon 2020 research and innovation programme (Grant Agreement No. 949120). This research was supported by the Scientific Service Units of The Institute of Science and Technology Austria (ISTA) through resources provided by the Miba Machine Shop. We thank the machine shop technical assistance of Ricardo Silva and Andrés Espinosa at Departamento de Física, Universidad de Chile.

-
- [1] P. Berdeklis and R. List, *J. Atmos. Sci.* **58**, 2751 (2001).
 - [2] R. Cocco, F. Shaffer, R. Hays, S. R. Karri, and T. Knowlton, *Powder Technol.* **203**, 3 (2010).
 - [3] D. Thorpe, S. Singh, P. Cartwright, and A. Bailey, *J. Electrostat.* **16**, 193 (1985).
 - [4] H. Liu, C. Cao, J. Huang, Z. Chen, G. Chen, and Y. Lai, *Nanoscale* **12**, 437 (2020).
 - [5] D. Posada, J. A. Jordan, A. Malik, A. Radulovic, J. J. Wang, S. Rhodes, C. Buhler, and T. Henderson, in *Proceedings of the SPIE 12121, Sensors and Systems for Space Applications XV* (SPIE, Orlando, Florida, 2022), p. 1212109.
 - [6] T. Steinpilz, K. Joeris, F. Jungmann, D. Wolf, L. Brendel, J. Teiser, T. Shinbrot, and G. Wurm, *Nat. Phys.* **16**, 225 (2020).
 - [7] J. F. Kok and N. O. Renno, *Phys. Rev. Lett.* **100**, 014501 (2008).
 - [8] C. Singh and M. G. Mazza, *Phys. Rev. E* **97**, 022904 (2018).
 - [9] M. Sow, E. Crase, J. L. Rajot, R. M. Sankaran, and D. J. Lacks, *Atmos. Res.* **102**, 343 (2011).
 - [10] J. S. Gilbert, S. J. Lane, R. S. J. Sparks, and T. Koyaguchi, *Nature* **349**, 598 (1991).
 - [11] H. Zhao, G. Castle, and I. Inculet, *J. Electrostat.* **55**, 261 (2002).
 - [12] S. R. Waitukaitis and H. M. Jaeger, *Rev. Sci. Instrum.* **84**, 025104 (2013).
 - [13] S. R. Waitukaitis, V. Lee, J. M. Pierson, S. L. Forman, and H. M. Jaeger, *Phys. Rev. Lett.* **112**, 218001 (2014).
 - [14] V. Lee, S. R. Waitukaitis, M. Z. Miskin, and H. M. Jaeger, *Nat. Phys.* **11**, 733 (2015).
 - [15] V. Lee, N. M. James, S. R. Waitukaitis, and H. M. Jaeger, *Phys. Rev. Mater.* **2**, 035602 (2018).
 - [16] J. Haerberle, A. Schella, M. Sperl, M. Schröter, and P. Born, *Soft Matter* **14**, 4987 (2018).
 - [17] F. Pertl, J. C. Sobarzo, L. Shafeek, T. Cramer, and S. Waitukaitis, *Phys. Rev. Mater.* **6**, 125605 (2022).
 - [18] G. Grosjean, S. Wald, J. C. Sobarzo, and S. Waitukaitis, *Phys. Rev. Mater.* **4**, 082602(R) (2020).
 - [19] G. Grosjean and S. Waitukaitis, *Phys. Rev. Lett.* **130**, 098202 (2023).
 - [20] R. Yoshimatsu, N. A. M. Araújo, G. Wurm, H. J. Herrmann, and T. Shinbrot, *Sci. Rep.* **7**, 1 (2016).
 - [21] T. Siu, J. Cotton, G. Mattson, and T. Shinbrot, *Phys. Rev. E* **89**, 052208 (2014).
 - [22] T. Pähz, H. J. Herrmann, and T. Shinbrot, *Nat. Phys.* **6**, 364 (2010).